Journal of Structural Geology, Vol. 12, No. 4, pp. 431 to 441, 1990
Printed in Great Britain

0191-8141/90 $03.00+0.00

Kinematic analysis of shear zones in sandstone and mudstone of the Shimanto belt, Shikoku, SW Japan

DARREL S. COWAN

Department of Geological Sciences, University of Washington, Seattle, WA 98195, U.S.A.

(*Received* 21 *July* 1989; *accepted in revised form* 4 *January* 1990)

Abstract—I describe kinematic criteria for sense-of-shear in unmetamorphosed interbedded sandstone and mudstone of the Tertiary Shimanto accretionary complex at Ariigawa, Kōchi Prefecture. In certain zones parallel to bedding and up to several meters wide, sandstone layers with internal bedding-parallel turbidite laminations are broken into blocky rectangular fragments or inclusions. Many inclusions rotated counterclockwise and so indicate a sinistral sense-of-shear with respect to the present orientation of bedding. Asymmetric folds corroborate this interpretation. Amounts of rotation are variable and are inversely proportional to the axial ratios of fragments. Fragments with axial ratios greater than about 4–6 did not rotate, while those with ratios between 4 and 1 record progressively greater maximum rotations. These observations accord with theoretical and experimental analyses describing the behavior of rigid inclusions in a matrix subjected to simultaneous simple shear and pure shear. The data from the Shimanto suggest that: (1) the rotation-inducing deformation included a coaxial component and departed from strictly non-coaxial simple shear; and (2) total shear strains were of the order of 3–5.

INTRODUCTION

Two questions naturally arise regarding mesoscopic zones of ductile or brittle deformation. The first, and more difficult, addresses whether the strain history was predominantly coaxial or non-coaxial. The second concerns the sense-of-shear or vorticity within zones of non-coaxial deformation ('shear zones'). In the past decade structural geologists have identified a number of criteria for sense-of-shear in ductile deformation zones, where strain at medium and high metamorphic grades is accommodated almost entirely by crystal-plastic, grain-scale deformation mechanisms (see review by Simpson & Schmid 1983). In some instances, workers (for example, Law 1987, Vissers 1989) have used crystallographic fabrics to infer departures from perfectly non-coaxial flow in some mylonitic zones.

Although deformation or movement zones are common in ancient, on-land accretionary wedges, they have so far resisted these kinds of kinematic analyses, largely because the deformation mechanisms operating in them were dominantly intergranular (particulate) and cataclastic flow (Knipe 1986). Moreover, much of the deformation in such zones and wedges is thought to have involved wet sediments under elevated fluid pressures at low, sub-greenschist or 'non-metamorphic' temperatures. In this paper, I present some kinematic criteria from shear zones in unmetamorphosed sandstone–mudstone turbidites in the Shimanto accretionary belt on Shikoku. Using some of these criteria, I will also propose that the deformation path within the zones was not strictly one of progressive simple shear but rather included a component of pure shear. The analysis is based partly on a theoretical and experimental study by Ghosh & Ramberg (1976), who analyzed the rotation and reorientation of rigid inclusions in a viscous matrix.

THE SHIMANTO BELT

Regional setting

The Shimanto belt (Fig. 1) constitutes the most oceanward tectonic element of southwest Japan. It consists predominantly of Cretaceous to Miocene interbedded sandstone and mudstone, and a small proportion of tectonically intercalated mafic volcanic rocks and radiolarian-rich chert and mudstone. Taira (1981), Taira *et al.* (1982, 1985), Suzuki & Hada (1983) and Ogawa (1985) provided recent overviews of the belt; Taira *et al.* (1980) contains important information about the Shimanto in Kōchi Prefecture on Shikoku. From the literature to date, it is clear that the Shimanto belt can be interpreted broadly as an uplifted, exposed accretionary wedge, comprising not only materials scraped off descending oceanic plates but probably slope-basin deposits

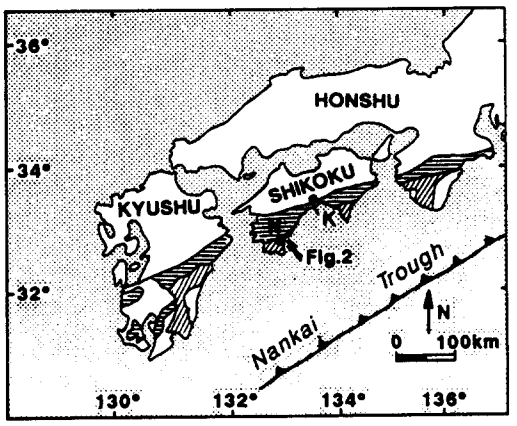

Fig. 1. Location map of SW Japan. Horizontal rules = Cretaceous part of the Shimanto belt; diagonal rules = Tertiary Shimanto belt. K = Kōchi; N = Nakamura.

as well. The Shimanto belt is presently contiguous with an offshore accretionary wedge that is actively growing oceanward as a result of subduction along the Nankai trough or trench (Fig. 1) (Aoki *et al.* 1982, Kawamura & Aoki 1986).

On Shikoku, the Shimanto displays some of the significant attributes of the belt as a whole. Strata typically strike ENE, parallel to the entire belt. They generally dip steeply northward, face northward, but become progressively younger (Cretaceous to early Miocene) southward, toward the Nankai trough. These observations, based largely on the literature cited above and on unpublished mapping by Taira and his co-workers, suggest that mappable formations or sequences have been imbricated along what are now steeply dipping reverse faults. At the mesoscopic scale, bedding in sequences of sandstone and mudstone ranges from intact and well preserved to strongly disrupted or folded. Sakai (1981), Ditullio & Byrne (1987), Hibbard & Karig (1987) and Agar (1988) describe some of the complicated small-scale structures on Shikoku and relate them to hypothesized processes of accretion.

Study area

I studied superb exposures on wave-cut platforms near Inomisaki (Ino Point), some 75 km SW of Kōchi and 9 km NE of Nakamura (Figs. 2 and 3). The Shimanto belt is nearly continuously exposed at low tide along the coast from Shirahama to Inomisaki and consists (Taira unpublished mapping) of E-striking, steeply N-dipping to vertical panels that are fault-bounded and range in thickness from about 200 to 500 m. Sandstone-rich panels are interspersed with sequences of interbedded sandstone–mudstone turbidites. The Shimanto here is probably largely Eocene on the basis of radiolarians recovered from minor lenses of hemipelagic red and green mudstones (Taira personal communication 1987). The boundary between the Paleogene and Cretaceous parts of the Shimanto is not well located in this area, however, so some of the section could be late Cretaceous. Layers of medium- to thick-bedded sandstone are typically continuous but tightly folded. Thin layers of sand in mudstone-rich sequences are commonly offset along small faults (Agar 1988), broken and pulled apart, or chaotically mixed with mudstone. I focused on certain outcrops west of the village of Ida in the Ariigawa district of Ōgata-chō (township) (Fig. 2), where rotated rectangular blocks derived from sandstone layers seemed amenable to a kinematic analysis. Another example of rotated blocks crops out on a wave-cut platform 1.9 km south of the hamlet of Shirahama (Fig. 2).

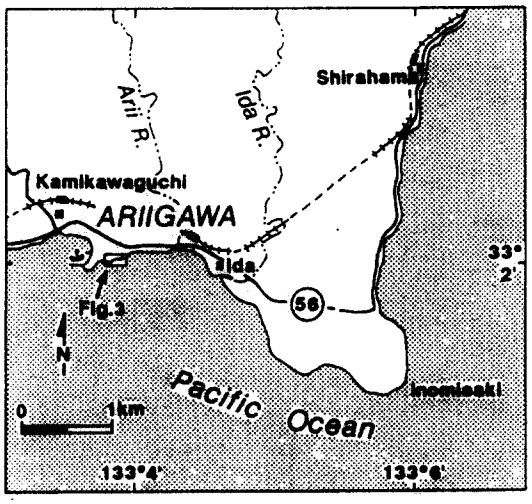

Fig. 2. Location map of Ariigawa district. Crossed line = railway; line is dashed through tunnels.

DISRUPTED STRATA IN THE STUDY AREA

Local setting

Figure 3 is a simplified, schematic geologic map of the study area in Ariigawa. The outcrops exposed at low tide here are easily accessible from either the highway (Route 56) or nearby stations on the railway (Fig. 2). Rocks at Ariigawa are exclusively sedimentary. Except where folded, bedding on average strikes about N10–22°E, dips 75–85°E, and faces consistently toward the east. The overall orientation of this sequence is notably different from that of the coastal section between Inomisaki and Shirahama; the Ariigawa block appears to have rotated clockwise about 110° relative to the E-striking, N-facing section at Shirahama. I identified several units in the study area on the basis of differences in rock type, bedding thickness, and deformational style (Fig. 3). Most of the units (2, 3, 5, 7–9) comprise interbedded sandstone and mudstone. Sections consisting of medium- to thick-bedded sandstone contain about 5% mudstone; thin-bedded sandstone is typically restricted to mudstone-dominated units. I interpret these

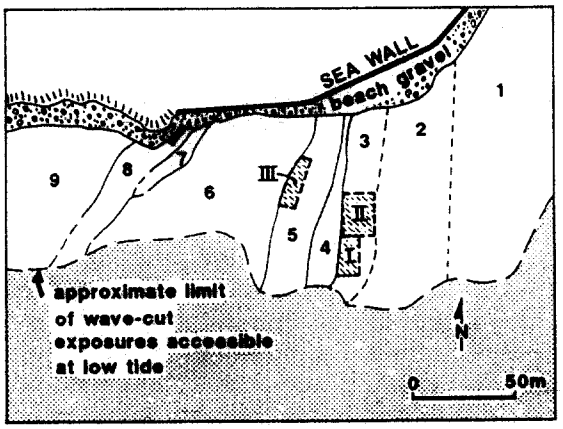

Fig. 3. Simplified geologic map, constructed on an air-photograph base, of the wave-cut bench that was studied in detail. Location is shown in Fig. 2. Details about some of the units are provided in the text. Units 1, 4 and 6 are dominantly greenish gray hemipelagic mudstone. Units 2 and 7 are dominantly medium-bedded sandstone. Units 3, 5 and 9 consist of about 80% mudstone and 20% thin-bedded sandstone. Unit 8 is thick-bedded sandstone. Contacts are dashed where approximately located. Data from domains I, II and III (dashed rectangular boxes) are displayed in Fig. 7.

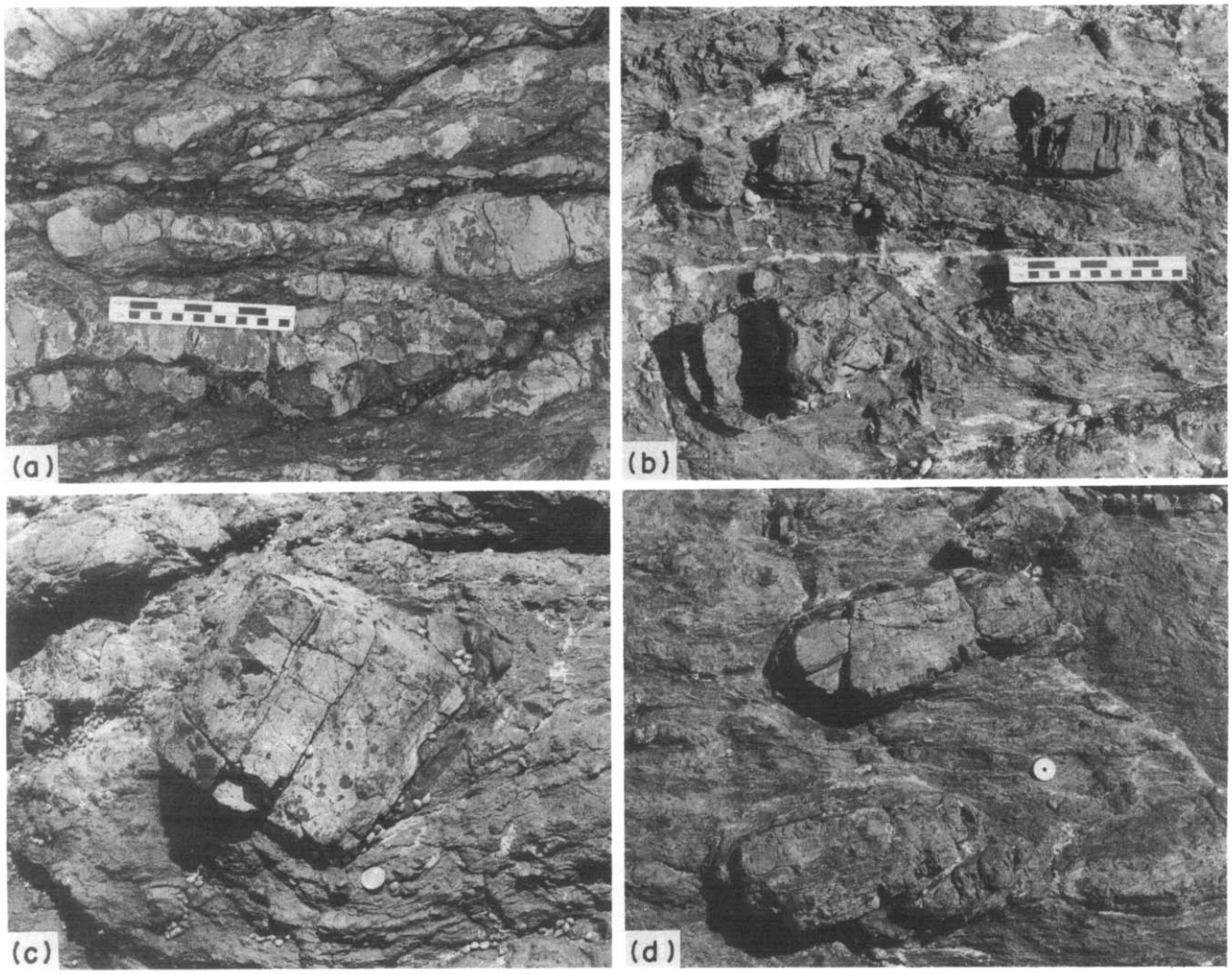

Fig. 4. (a) Sandstone turbidites and interbedded mudstone in Unit 9. Sandstone layers are variably extended and typically lenticular rather than blocky. Note absence of internal laminations in beds and fragments of sandstone. (b) Rectangular blocks, derived from internally laminated layers of sandstone, in unit 3. (c) & (d) Two examples of rectangular blocks in unit 3 that have rotated counterclockwise. Compare with idealized inclusions in Fig. 6. Photographs taken facing ESE, normal to bedding, and looking directly down onto the wave-cut bench. Undisrupted beds, from which fragments like these were derived, strike generally N10°E (horizontally in the photographs), are vertical and face east. Note that the weak fissility in the enclosing mudstone is parallel to the sheet-dip of bedding and thus horizontal in the photographs. Inclusions display well-preserved internal laminations. In (c) R (axial ratio) = 1.05; φ = 147°; coin diameter = 22 mm. In (d) top, R = 2.8; φ = 105°; bottom, R = 2.5; φ = 105°; coin diameter = 20 mm.

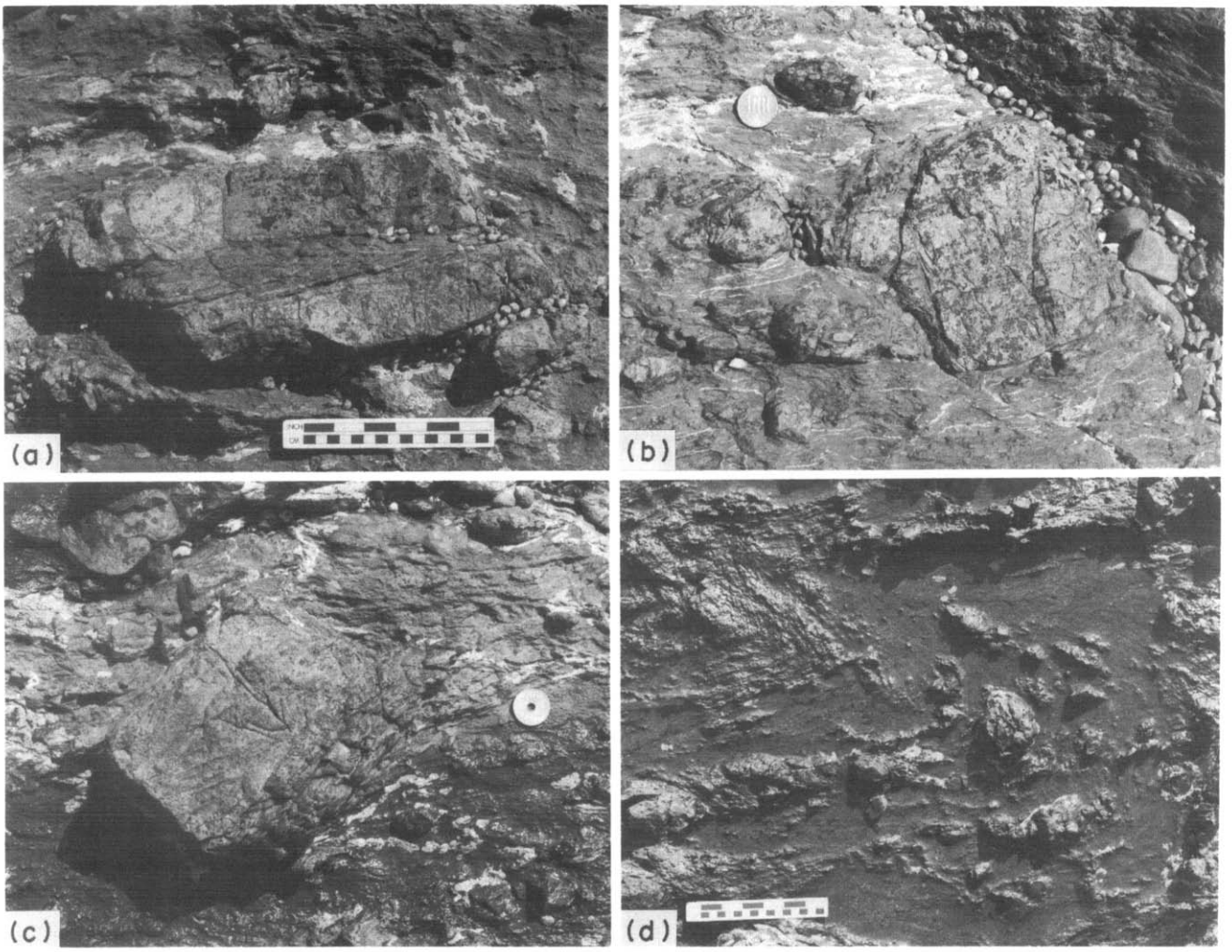

Fig. 5. Inclusions in unit 3 that record distortion as well as rotation. All photographs taken facing east, looking directly down on wave-cut bench; undisrupted sandstone beds and fissility in mudstone are horizontal in photographs. (a) Fragment displays sinistral slip along a thin layer of mudstone between two sandstone beds; entire fragment records small counterclockwise rotation. (b) & (c) Tails or wings of sand that were drawn away from fragments. Coin diameter in (b) 20 mm; in (c) 22 mm. (d) Profile view (photograph made facing east; undisrupted bedding would be oriented horizontally in photograph) of a vertically plunging, S-shaped fold in unit 3. Folding postdated the formation of sandstone fragments and of fissility in mudstone. Overall sense of shear is sinistral.

interbedded sequences as turbidites but am unable to pinpoint their depositional setting (e.g. trench vs trench-slope basin). The greenish gray mudstone in units 1, 4 and 6 (Fig. 3), containing rounded to lenticular fragments of buff chert up to 10 cm in diameter, is probably hemipelagic. The units themselves and the contacts between them are oriented roughly parallel to bedding, and there is no evidence in the limited exposures for folding on the scale of the entire study area depicted in Fig. 3.

Deformational styles

There are four prominent styles of mesoscopic deformation represented in the study area, but I investigated only one of them (see 4 below) in detail.

(1) Steeply plunging, moderately to tightly appressed folds with average amplitudes of 0.5–3 m are developed in the medium-bedded sandstone of units 2 and 7. Such folds typify medium-bedded sandstones between Shirahama and Inomisaki as well.

(2) In the northern part of unit 2, the proportion of mudstone is greater than in the sandier facies to the south. Folds have irregular shapes and are interspersed with a 'blocky mudstone' containing chaotically disposed, variably shaped fragments of sandstone, some of which are remnants of folds. Mud or mudstone appears to have been highly mobile and invasive during deformation.

(3) Unit 9 originated as a sequence of thin- to medium-bedded sandstone turbidites interlayered with mudstone. Most of the sandstone beds have undergone layer-parallel extension. Although the continuity and orientation of bedding are obvious in outcrop, on a smaller scale individual beds display a variety of extensional structures ranging from pinch-and-swell to complete boudinage (Fig. 4a). Lenticular fragments are common, and overall, extension was accommodated by mesoscopically ductile flow, rather than brittle fracture, of the sand or sandstone. All evidence points to omnidirectional extension in the plane of the layering. This style of deformation is common in subduction complexes; Cowan (1985) described rock units so deformed as 'type I melange'. (Note that this use of *melange* differs from how most Japanese workers use the term in the Shimanto; they reserve it for tectonic mixtures including oceanic basalt and chert in addition to deformed sandstone and mudstone.)

(4) The deformed rocks that were the focus of my study constitute most of unit 3 and part of 5. They are also characterized by a 'blocky' fabric, but the fragments of sandstone layers are rectangular, rather than lenticular, in cross-section (Fig. 4b). Compared to the other units in this part of the Shimanto belt, two attributes of unit 3 make it uniquely suited for a kinematic analysis: many of the fragments have rotated, and nearly all of the thin sandstone beds and fragments are finely laminated. These turbidite T_{bc} laminations serve as an internal datum that one can use to compare the orientations of beds and fragments. In contrast, the fragments in unit 9 are devoid of laminations, and only a few show unequivocal evidence for rotation.

KINEMATIC ANALYSIS

Before presenting the kinematic criteria in disrupted strata of units 3 and 5, I want to summarize briefly some pertinent results from Ghosh & Ramberg (1976). They theoretically analyzed the rotation of rigid inclusions in a viscous matrix subjected to simultaneous simple shear and shortening normal to the shear plane. The geometry of their idealized, rotating inclusion is illustrated in Fig. 6 for the case of sinistral shear. Note that the deformation is a plane strain. The axis of rotation coincides not only with one of the three orthogonal axes of the inclusion, but also with the *Y*-axis of the bulk strain ellipsoid. Hence, the inclusion does not rotate out of the plane of the figure, which is the *XZ* plane of bulk strain.

Ghosh & Ramberg (1976) showed that the behavior of an inclusion, expressed as its rate and sense of rotation, is a function of its orientation (ϕ_o in Fig. 6), axial or aspect ratio (R) and the 'strain-rate ratio' (s_r), or ratio between the rates of natural strain (elongation) in the shear plane (parallel to the x-co-ordinate axis in Fig. 6) and shear strain. In cases where $s_r = 0$ (exclusively non-coaxial strain paths), as γ (shear strain) progressively increases, all inclusions with $R \geq 1$ will rotate continuously, but at different rates, in the direction expected from the sense of shear (sinistral, hence counterclockwise, in Fig. 6). The only exceptions, of course, are passive markers or inclusions with very high aspect ratios, which have a rotation rate of zero when they lie parallel to the shear plane (x direction). The effect of progressively increasing s_r—increasing the component of pure shear—is to suppress the rotation of inclusions with progressively smaller aspect ratios. In other words, only inclusions with R less than a critical value (depending on s_r) rotate continuously; more elongate inclusions rotate significantly more slowly and eventually come to rest. For some cases, where $s_r > 0$ (see Ghosh & Ramberg 1976, for details), certain inclusions will in

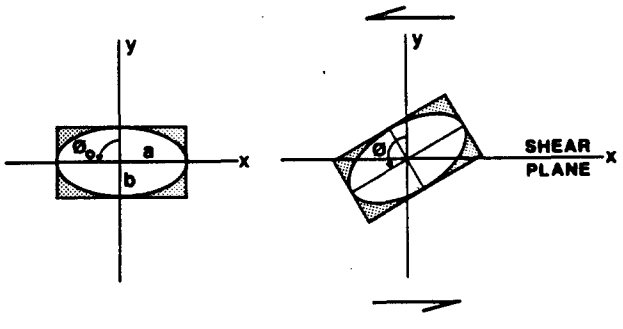

Fig. 6. Geometry of an idealized rigid inclusion rotating in a counterclockwise sense in response to sinistral shear strain in its enclosing matrix (modified from fig. 1 of Ghosh & Ramberg 1976). See text for discussion. Both an ellipsoid and a rectangular inclusion with the same axial or aspect ratio (a/b) are shown. ϕ_o = initial (pre-rotation) orientation, expressed as the angle between the y-axis (normal to shear plane) and the a-axis of the inclusion. ϕ = final (after rotation) angle between y-axis and a-axis of the inclusion.

theory rotate 'backwards', in the opposite sense expected from the sense of shear. This latter behavior is a warning that sense of rotation is not an infallible criterion for sense of shear, unless ϕ_o and s_r are independently known or estimated.

Kinematic criteria in disrupted strata of units 3 and 5

Rotated inclusions. Unit 3 consists of about 80% light- to dark-gray mudstone and 20% sandstone. Most sandstone beds are 10 cm or less in thickness. Some are continuous for up to 10 m, but fragments of diverse shapes and sizes that were derived from beds predominate. Most of unit 3 has a decidedly 'blocky', rather than bedded, appearance. Continuous beds strike N16–6°E, dip 75°E to vertically, and face east. (Cross-laminae and rare graded bedding are facing criteria.) Mudstone has a weak, irregular fissility that is oriented roughly parallel to bedding. This fabric is evident in Figs. 4(c) & (d) and is most easily visible on dry wave-cut surfaces or in hand-specimens that break apart parallel to it.

A small proportion—probably less than 10%—of the fragments are obviously significant kinematically: they are square to rectangular in three dimensions and contain T_{bc} laminae that are parallel to their long axes. Many have apparently rotated, because their laminae and bounding bedding surfaces are no longer parallel to the average orientation of bedding (the 'sheet-dip') in the unit (Figs. 4c & d). Notably, the rotations can be referred to a single axis, lying within bedding with a pitch of 90°. This fortuitous circumstance means that these fragments, when viewed in the horizontal cross-section provided by the wave-cut bench, are analogous to the idealized rotating inclusion in Fig. 6. Moreover, these inclusions rotated apparently in response to a bulk strain affecting both matrix and inclusions. The rotations were not induced by slip along extensional shear fractures oriented oblique to layering (see, for example, Needham 1987). Therefore, the rotations are amenable to a Ghosh–Ramberg analysis (for example, compare Figs. 4c & d with Fig. 6).

In the field, I selected three domains (located in Fig. 3; two are in unit 3 and one is in a lithologically and structurally similar part of unit 5) of about 80—100 m^2 each and measured the amounts of apparent rotation of square and rectangular, laminated fragments, for which I could easily determine an aspect ratio. Results appear in Fig. 7. The conventions used for measurements were as follows. All measurements were made facing east. The angle between the internal lamination in a fragment, and the average orientation of bedding (sheet-dip) in the domain was added to 90° if the fragment appeared to have rotated counterclockwise, and subtracted from 90° if clockwise. This convention implicitly assumes that internal laminations, and hence rectangular fragments, were initially parallel to bedding ($\phi_o = 90°$) before rotation, and that the plane of bulk shear was approximately parallel to bedding. These assumptions are defended below. Figure 7 shows that an overwhelming majority of the fragments rotated counterclockwise. Also, the results accord with the simple prediction of Ghosh & Ramberg (1976) that, for strain paths dominated by progressive simple shear ($0 \leq s_r \leq 1$) and for $\phi_o \approx 60$–90°, shorter fragments or inclusions rotate faster than longer ones. Stated another way, for any given γ imposed uniformly throughout a domain, shorter inclusions rotate progressively more than longer ones.

I interpret the counterclockwise rotations to have occurred in response to bulk sinistral shear (with respect to present orientation of bedding, facing east) in units 3 and 5. This conclusion depends on three assumptions. First, I assume that the plane of bulk shear was approximately parallel to bedding. Bedding imparts a strong mechanical anisotropy to the section on the scale of the smaller domains and on the scale of the exposure at Ariigawa as a whole. I infer that this anisotropy not only localized strain but also ensured that slip would occur parallel to it. There is no evidence, for example, of deformation zones, containing fragments of disrupted beds, that cut across the contacts between units mapped in Fig. 3. The second assumption is that the shear direction or slip line was approximately horizontal, with respect to the present orientation of bedding. Less than 5% of the hundreds of laminated fragments I examined appeared to have rotated about anything other than a vertical axis (with respect to present orientation of bedding). Whether the deformation was a plane strain does not affect conclusions about sense of shear, but it may bear on interpretations of the strain path, presented below.

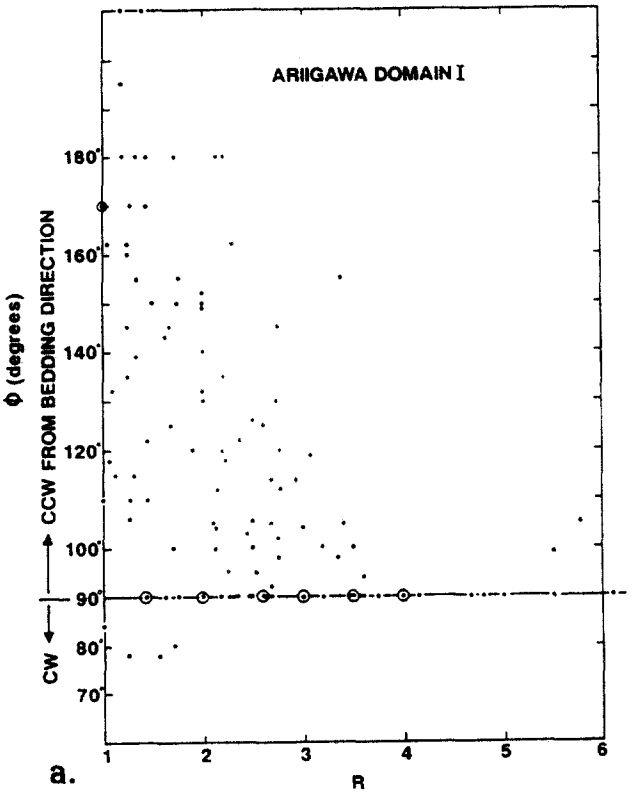

Fig. 7(a).

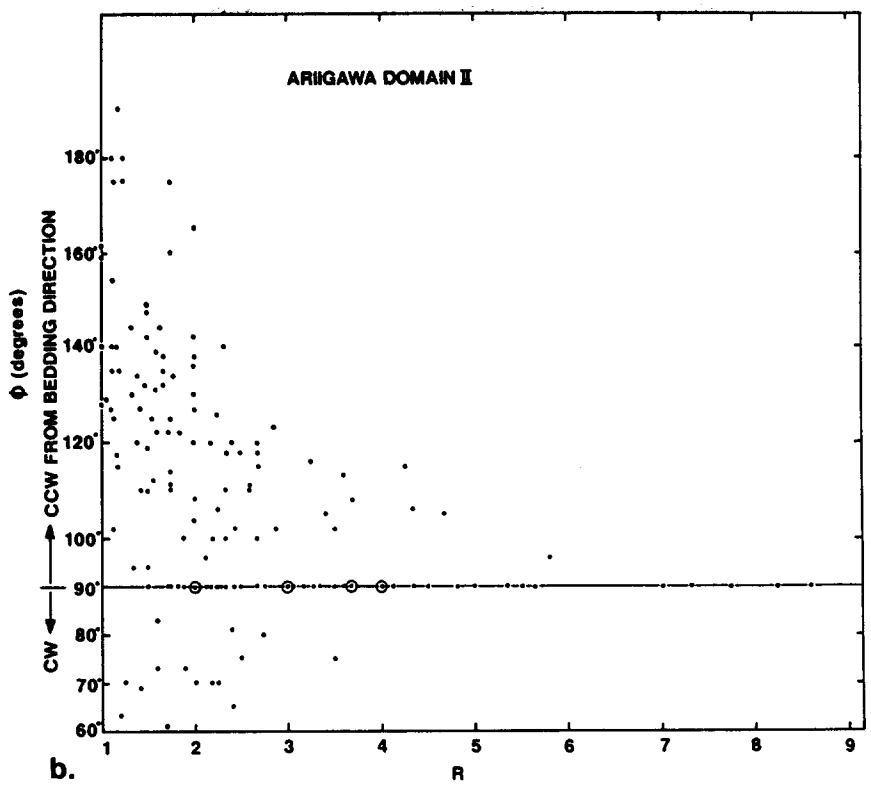

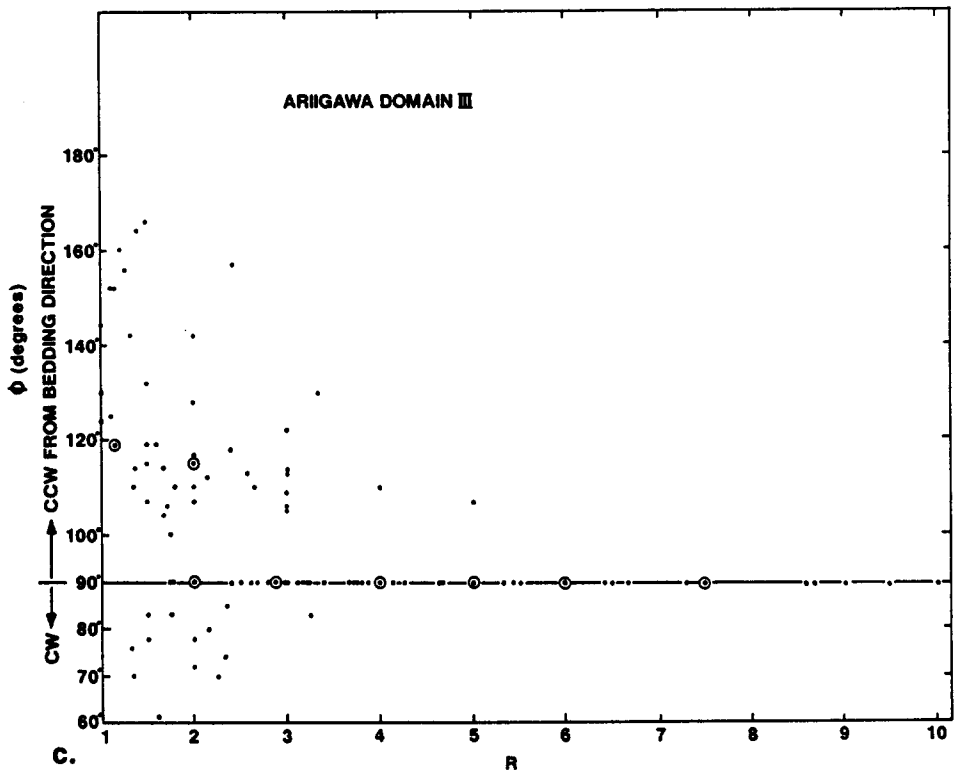

Fig. 7. Graphs depicting ϕ, the angle between internal laminations in fragments of sandstone and the normal to bedding in undisrupted sandstone layers, plotted against R, the axial ratio (a, the long axis, is parallel to internal laminations; b is normal). See Fig. 6 for a geometrical representation of these parameters. $\phi = 90°$ is the orientation of undisrupted bedding and of fragments that have apparently not rotated. Fragments with $\phi > 90°$ have apparently rotated counterclockwise (CCW); those with $\phi < 90°$ have apparently rotated clockwise (CW). Circled points = two fragments, each with same ϕ and R. (a) Domain I; (b) domain II; (c) domain III (see Fig. 3 for location of domains).

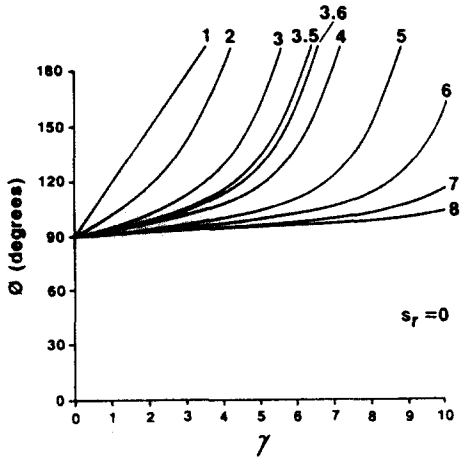

Fig. 8. Graphical solutions to equations (11), (12) and (13) in Ghosh & Ramberg (1976). See text for discussion. $s_f = 0$; $\phi_o = 90°$. Curves shown are for different axial ratios, R. γ = shear strain. ϕ is defined in Fig. 6.

The third assumption is that most fragments had an initial orientation $\phi_o = 90°$, parallel to both bedding and the shear plane, prior to the rotation-inducing deformation. This initial state is only one of several possibilities, which can be evaluated while contemplating Figs. 7 and 8. Figure 8 shows how the initial orientation and axial ratio of an inclusion influences its rotational behavior. Inclusions with a range of aspect ratios are depicted for comparison with Fig. 7. For the present, we need only consider behavior where $s_r = 0$. For the case favored here, consider that all inclusions, with $1 \leq R < 10$, were originally oriented parallel to bedding—that is $\phi = 90°$ in Fig. 7. As γ progressively increased, inclusions should have rotated at rates inversely proportional to their aspect ratios. If each inclusion was subjected to the same γ and rotated according to Fig. 8, the final orientations should plot along lines of negative slope on graphs with axes ϕ and R. (The slopes and intercepts of the lines would depend on s_r.) Instead, the final orientations as observed in all domains (Fig. 7) exhibit a different pattern. Inclusions with aspect ratios less than a certain value of R_m (~3.8 in domain I; ~6 in II and III) appear to have rotated variable amounts. Several inclusions with $R < R_m$ have $\phi = 90°$, and appear not to have rotated at all. A few have $\phi < 90°$, and appear to have rotated in a clockwise sense or 'backwards'.

I interpret the pattern in Fig. 7 as follows. In a set of inclusions with any given R and $\phi_o \approx 90°$, only a small percentage were able to achieve the maximum predicted counterclockwise rotation; the remainder were variably retarded. Some did not rotate at all, and these have $\phi = 90°$ in Fig. 7. The inclusions that plot below the abscissa in Fig. 7 might originally have had $60° < \phi_o < 90°$. Each of these is also interpreted to have variably rotated in a counterclockwise sense, such that its ϕ plots somewhere between its ϕ_o and its maximum predicted rotation. This model of 'retarded rotations' is based on the premise that, within each of the domains represented in Fig. 7, both γ and s_r were approximately constant rather than locally variable, from inclusion to inclusion, on the scale of cm.

Alternative initial states were much less likely, in my opinion. For example, if inclusions with $R < 10$ had had completely random initial orientations, the points in Fig. 7 would have been more widely scattered above and below the abscissa for all values of R. If all inclusions had initially been oriented obliquely (say ϕ_o 70°), then the modest shear strains ($\gamma \leq 4$) that were required to achieve the maximum rotations in Fig. 7 for $R < 3.8$ would have been insufficient to achieve the observed $\phi = 90°$ in inclusions with $R > 3.8$. As for the inclusions with $\phi < 90°$, it is possible that some or all rotated clockwise (dextrally) from $\phi_o = 90°$.

Distorted inclusions. A few originally rectangular inclusions are distorted; they probably changed shape during rotation. We can compare their shapes with those of porphyroclasts and broken grains in mylonitic shear zones, even though the deformation mechanisms (intergranular flow and crystal-plasticity, respectively) are utterly different. The fragment in Fig. 5(a) records counterclockwise rotation, and sinistral slip along internal bedding planes. Some inclusions have tails or wings oriented parallel to the crude foliation in the matrix (Figs. 5b & c). The tails consist of sand grains and fragments that were derived and drawn away from the adjacent inclusion. The example in Fig. 5(b) displays the geometry conventionally associated with sinistral shear and counterclockwise rotation in shear zones in metamorphic rocks (compare fig. 4A in Simpson & Schmid 1983). Otherwise inclusions show seemingly contradictory kinematic criteria. In Fig. 5(c) for example, the sandstone block appears to have rotated counterclockwise (sinistral shear), but the tail is disposed as if dextral shear had occurred. Until we accumulate further observations on the geometry of tails and bedding-plane slip in similar deformed unmetamorphosed rocks, these particular kinematic criteria should be used with caution.

Folds. Locally in units 3, 5 and 8, the planar fabric defined by elongate inclusions (fragments of beds), continuous and pulled-apart bedding, and the crude bedding-parallel fissility in mudstone is folded (Fig. 5d). These asymmetric folds typically occur in isolation rather than in trains, are moderately to steeply plunging (Fig. 9), and have wavelengths averaging about 0.5 m. When they are viewed facing east, these folds invariably are S-shaped in profile. Their geometry is compatible with, and thus independently supports, the hypothesis of sinistral shear that is based on rotated inclusions. The folds record a more localized and probably later response to the bulk sinistral deformation than do the more widely distributed, rotated inclusions. The variable plunge (Fig. 9) may represent the passive rotation of originally steeply plunging hinges toward the direction of maximum bulk elongation (X of the bulk-strain ellipsoid), which is interpreted to trend approximately parallel to the strike of layering (NNE–SSW).

Folds are common in the medium- to thick-bedded

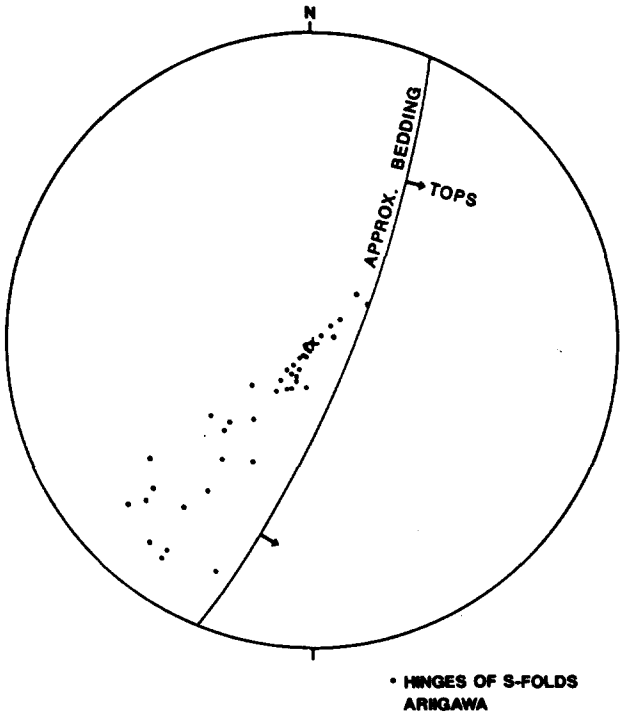

Fig. 9. Hinges of asymmetric S-folds, of the type shown in Fig. 5(d), in units 3, 5 and 8. Hinges are apparently dispersed in a partial girdle and might have rotated from an initial dominantly vertical plunge. The girdle depicted represents ESE-facing bedding striking N22°E and dipping 80°E; actual measured values of strike and dip range from N–S and 90° to this value.

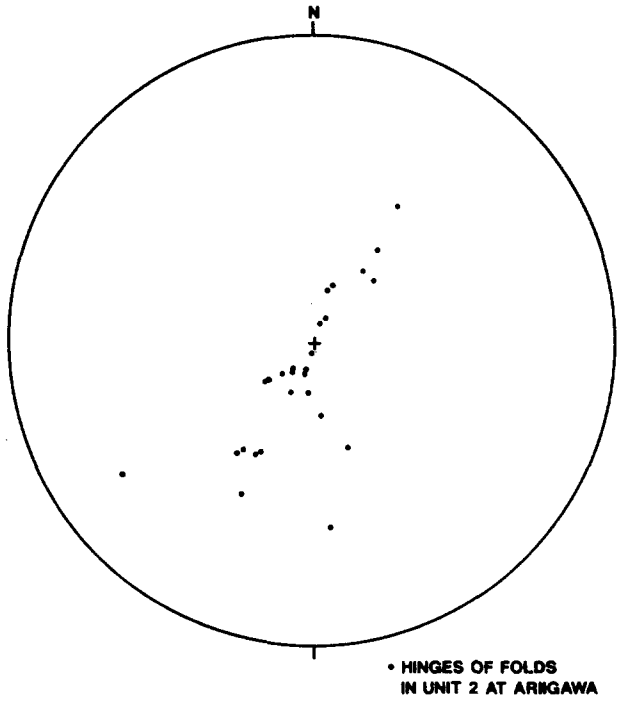

Fig. 10. Hinges of folds in medium-bedded sandstone of unit 2. See text for discussion.

sandstones of units 2 and 7; unit 2 is adjacent to unit 3 containing the shear zones discussed above (Fig. 3). The folds in 2 and 7 are typically symmetric, occur in trains, and are notably larger than the asymmetric folds that deform disrupted strata in units 3, 5 and 8; the average amplitude is probably 1–3 m. Most hinges plunge steeply (Fig. 10), but they are dispersed along the same girdle that statistically encompasses most of the hinges of the asymmetric folds in the shear zones (Fig. 9). In units 2 and 7, however, the folds plunge NE as well as SW.

Overall kinematic interpretation

I interpret the rocks exposed on the wave-cut terrace at Ariigawa as a variably deformed, E-facing stratigraphic section. It comprises a succession of diverse units that originally differed from one another on the basis of sand–mud ratios and the average thickness of sand layers. I suggest that the zones consisting largely of disrupted strata—variably extended beds and isolated fragments of beds—are movement or shear zones, and that the sense of shear in at least some of them was sinistral. On a mesoscopic scale, the mean ductility of the mud or mudstone was high, and elevated fluid pressures ("wet-sediment deformation" of Pickering 1987) might well have influenced the behavior of mud and sand. Although the deformation is stratigraphically localized, the lithologic units themselves, some distinctive beds within them, and the contacts separating them are continuous and parallel on the scale of the study area (Fig. 3). Because there is no evidence for higher strain (more fragmentation, more intensive foliation, greater rotations) at lithologic contacts, I discount the hypothesis that the observed deformation was localized along faults that duplicated or excised section. Whether the shear zones formed in domains of layer-parallel slip on the limbs of macroscopic folds is more difficult to establish. Agar (1988) described dm-scale folds at Inomisaki (Fig. 2), but there is no map evidence for folds of this scale or larger in the admittedly restricted study area. A simple interpretation of the disrupted rocks at Ariigawa is that they record layer-parallel, laminar flow along décollements or transcurrent faults in partly consolidated, or 'wet', sediments.

STRAIN HISTORY

The rocks at Ariigawa illustrate how rotated inclusions may serve as a criterion for the sense of shear or vorticity in movement zones. Ghosh & Ramberg (1976), Hanmer (1984), Passchier (1987) and Vissers (1989) pointed out that rotated inclusions are potentially useful for addressing another question about shear zones: whether the deformation departed from simple shear (i.e. the 'IBM card-deck model'). Establishing the strain path or deformation history in terms of departures from non-coaxiality (e.g. Sanderson 1982, Platt & Behrmann 1986) or partitioning of coaxial and non-coaxial progressive strain (e.g. Lister & Williams 1983) may shed light on the tectonic setting of the shear zones in question. The setting of shear zones in sediments thought to have been deformed in or on accretionary prisms is currently controversial. Arguments invoking interpreted strain paths have been used to support defor-

mation along and beneath the décollement at the base of a prism (e.g. Fisher & Byrne 1987) or in gravitationally collapsing masses on or at the toe of a prism (e.g. Cowan 1982).

The following analysis of the strain history ("strain regime" of Hanmer 1984) utilizes Ghosh & Ramberg (1976) and the data from Ariigawa in Fig. 7. Ghosh & Ramberg (1976) emphasize that their mathematical analysis of progressive strain is rigorously applicable only to rigid ellipsoidal inclusions engulfed in a mesoscopically ductile matrix subjected to plane strain. In principle, however, their results should qualitatively apply to blocky, rectangular inclusions, such as those derived from sandstone beds in the Shimanto. Another assumption in the following analysis is that the ratio of the components of simple and pure shear was time-constant; Vissers (1989) presented examples of how observed rotations could be produced by time-constant or changing ratios of shear-strain rates. Accordingly, the interpretations about strain history presented below are approximate and speculative.

Figure 11, like Fig. 8, shows graphical solutions to equations (11), (12) and (13) in Ghosh & Ramberg (1976). In each case, $\phi_o = 90°$. These graphs illustrate the theoretically predicted maximum rotation of inclusions of diverse axial ratios (R) as shear strain (γ) progressively increases. Figure 8 depicts behavior in the strictly non-coaxial case ($s_r = 0$). Figures 11(a) & (b) depict rotations as the strain includes a progressively greater coaxial component ($s_r = 0.15$ and 0.3, respectively). Note that as s_r increases, the rotations of inclusions with progressively smaller axial ratios are retarded. For example, for a shear strain of 4 and $s_r = 0$, only inclusions with $R < 7$ will rotate more than 5°; for $s_r = 15$, only those with $R < 6$; and for $s_r = 0.3$, only those with $R < 4$.

Now consider the observed behavior of inclusions at Ariigawa as illustrated in Fig. 7. In each domain, there is a notable difference in the behavior of inclusions smaller than a certain axial ratio (R_m): about 3.8 in domain I (Fig. 7a); 6 in domain II (Fig. 7b); and about 5–6 in domain III (Fig. 7c). Inclusions with $R > R_m$ did not rotate; those with $R < R_m$, as discussed above in the section entitled "Rotated Inclusions", rotated variably. For any R, it is not known whether the maximum rotations depicted in either Figs. 7(a), (b) or (c) are the maximum possible theoretically, so the change in behavior, rather than amounts of rotation, is considered the more significant parameter.

A comparison of Figs. 7 and 11 permits the hypothesis that the strain path in the shear zones at Ariigawa was not strictly simple shear. Rather, it included a component of shortening across, and stretch subparallel to, the shear plane. If blocky inclusions indeed behave like their ellipsoidal counterparts with the same axial ratios, then s_r probably lies between 0.15 and 0.3. If the maximum rotations plotted in Fig. 7 are indeed the theoretically predicted maxima according to Fig. 11, then the shear strain responsible for the rotations in the shear zones is on the order of 3, and definitely less than 5.

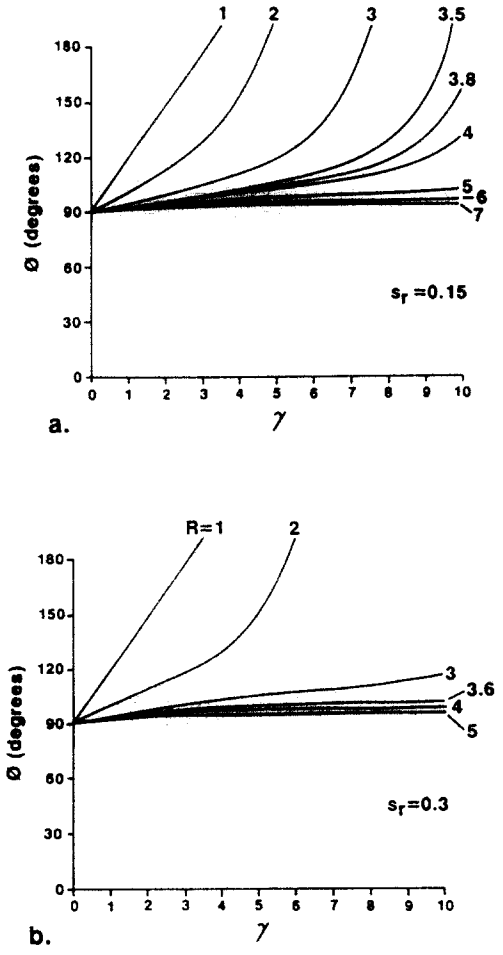

Fig. 11. Graphical solutions for equations (11), (12) and (13) in Ghosh & Ramberg (1976). (a) $s_r = 0.15$; (b) $s_r = 0.3$. See Fig. 8 for $s_r = 0$. Curves shown are for different axial ratios, R. γ = shear strain; ϕ is defined in Fig. 6.

Certain aspects of the total deformational history of the shear zones at Ariigawa are still unclear. If the assumption that $\phi_o \approx 90°$ for most inclusions is correct, then prior to the rotation-inducing deformation: (1) sandstone layers had already broken apart along extension fractures normal to bedding to form rectangular inclusions; and (2) the long axes of the inclusions either remained parallel to undeformed bedding, or, if the inclusions rotated, they were subsequently re-oriented to $\phi_o \approx 90°$. It seems that some or all of the early deformation was strongly coaxial; otherwise, equant ($R = 1$) inclusions would have rotated. The strain path, magnitude of strain, and setting of this early but cryptic deformation are unresolved.

Likewise, the setting and even the attitude of the shear zones when the inclusions rotated are a matter of speculation. The shear zones might have been related to low-angle thrust faults or the basal décollement near the toe of the early Tertiary Shimanto accretionary prism. Alternatively, they might have originated after the Shimanto strata had become nearly vertical, perhaps as the panel encompassing Ariigawa rotated clockwise from

the regional E–W strike. The kinematic criteria described and interpreted in this study are only part of the observational evidence needed to test these and other possibilities. Further investigations are also warranted to explain the extraordinary variety of mesoscopic structural styles in the Shimanto on SW Shikoku, even in areas separated by only a kilometer or so (compare this study with Agar 1988). The kinematic interpretations presented here apply strictly to the deformation zones at Ariigawa.

CONCLUSIONS

NNE-striking, steeply E-dipping and E-facing strata of the Shimanto belt at Ariigawa include bedding-parallel movement or shear zones. Within these, thin sandstone turbidites have broken into rectangular inclusions with diverse axial ratios. Some of these inclusions rotated in a sense indicating counterclockwise vorticity, or sinistral shear, with respect to the present orientation of bedding. Rotations accord in sense and magnitude with the theoretical and experimental analyses of Ghosh & Ramberg (1976), which predict progressively greater rotations for inclusions with progressively smaller axial ratios. While the utility of rotated inclusions as a criterion for sense of shear seems well established, their patterns of rotation also lead to more speculative conclusions about the strain path and magnitude of shear strain. At Ariigawa, the strain path apparently departed from ideal non-coaxial laminar flow (progressive simple shear), and included a component of pure shear. Shear strains (γ) for the part of the total deformation that induced rotations were probably on the order of 3.

Acknowledgements—I am deeply grateful for the kindness and hospitality of many Japanese colleagues and friends, without whose help this research could not have been accomplished. Yujiro Ogawa and Asahiko Taira introduced me to the Shimanto and the geology of SW Japan in general, and Hiroaki Matsugi at Kōchi University was instrumental in arranging logistics. Tim Byrne, Lee Ditullio, Jim Hibbard, and Dan Karig shared many of their observations and ideas on the Shimanto on Shikoku with me. I thank Ed Mulligan and Bill Bruner for writing the computer programs used to generate the graphs in Figs. 8 and 12. This research was supported by NSF Grant EAR-8506821.

REFERENCES

Agar, S. M. 1988. Shearing of partially consolidated sediments in a lower trench slope setting, Shimanto Belt, SW Japan. *J. Struct. Geol.* **10**, 21–32.

Aoki, Y., Tamano, T. & Kato, S. 1982. Detailed structure of the Nankai trough from migrated seismic sections. In: *Studies in Continental Margin Geology* (edited by Watkins, J. S. & Drake, C. L.). *Mem. Am. Ass. Petrol. Geol.* **34**, 309–322.

Cowan, D. S. 1982. Deformation of partly dewatered and consolidated Franciscan sediments near Piedras Blancas Point, California. In: *Trench–Forearc Geology* (edited by Leggett, J. K.). *Spec. Publs geol. Soc. Lond.* **10**, 439–457.

Cowan, D. S. 1985. Structural styles in Mesozoic and Cenozoic mélanges in the western Cordillera of North America. *Bull. geol. Soc. Am.* **96**, 451–462.

Ditullio, L. & Byrne, T. 1987. The role of out-of-sequence thrusting in the development of accretionary prisms: an example from the Eocene Shimanto belt, SW Japan. *Geol. Soc. Am. Abs. w. Prog.* **19**, 644.

Fisher, D. & Byrne, J. 1987. Structural evolution of underthrusted sediments, Kodiak Islands, Alaska. *Tectonics* **6**, 775–793.

Ghosh, S. K. & Ramberg, H. 1976. Reorientation of inclusions by combination of pure shear and simple shear. *Tectonophysics* **34**, 1–70.

Hanmer, S. K. 1984. The potential use of planar and elliptical structures as indicators of strain regime and kinematics of tectonic flow. *Geol. Surv. Pap. Can.* **81-1B**, 133–142.

Hibbard, J. & Karig, D. E. 1987. Sheath-like folds and progressive fold deformation in Tertiary sedimentary rocks of the Shimanto accretionary complex, Japan. *J. Struct. Geol.* **9**, 845–857.

Kawamura, T. & Aoki, Y. 1986. The Nankai trough margin, record 55-8. In: *Seismic Images of Modern Convergent Margin Tectonic Structure* (edited by von Huene, R.). *Am. Ass. Petrol. Geol. Studies in Geology* **26**, 54–56.

Knipe, R. J. 1986. Deformation mechanism path diagrams for sediments undergoing lithification. In: *Structural Fabrics in Deep Sea Drilling Project Cores From Forearcs* (edited by Moore, J. C.). *Mem. geol. Soc. Am.* **166**, 151–160.

Law, R. D. 1987. Heterogeneous deformation and quartz crystallographic fabric transitions: natural examples from the Moine thrust zone at the Stack of Glencoul, northern Assynt. *J. Struct. Geol.* **9**, 819–833.

Lister, G. S. & Williams, P. F. 1983. The partitioning of deformation in flowing rock masses. *Tectonophysics* **92**, 1–33.

Needham, D. T. 1987. Asymmetric extensional structures and their implications for the generation of melanges. *Geol. Mag.* **124**, 311–381.

Ogawa, Y. 1985. Variety of subduction and accretion processes in Cretaceous to Recent plate boundaries around southwest and central Japan. *Tectonophysics* **112**, 493–518.

Passchier, C. W. 1987. Stable positions of rigid objects in non-coaxial flow—a study in vorticity analysis. *J. Struct. Geol.* **9**, 679–690.

Pickering, K. T. 1987. Wet-sediment deformation in the Upper Ordovician Point Leamington Formation: an active thrust-imbricate system during sedimentation, Notre Dame Bay, north-central Newfoundland. In: *Deformation of Sediments and Sedimentary Rocks* (edited by Jones, M. E. & Preston, R. M. F.). *Spec. Publs geol. Soc. Lond.* **29**, 213–239.

Platt, J. P. & Behrmann, J. H. 1986. Structures and fabrics in a crustal-scale shear zone, Betic Cordillera, SE Spain. *J. Struct. Geol.* **8**, 15–33.

Sakai, H. 1981. Olistostrome and sedimentary mélange of the Shimanto terrane in the southern part of the Muroto Peninsula, Shikoku. *Sci. Rep. Dept Geol. Kyushu Univ.* **14**, 81–101.

Sanderson, D. J. 1982. Models of strain variation in nappes and thrust sheets: a review. *Tectonophysics* **88**, 201–233.

Simpson, C. & Schmid, S. M. 1983. An evaluation of criteria to deduce the sense of movement in rocks. *Bull. geol. Soc. Am.* **94**, 1281–1288.

Suzuki, T. & Hada, S. 1983. Accretionary melange of Cretaceous age in the Shimanto belt in Japan. In: *Accretion Tectonics in the Circum-Pacific Regions* (edited by Hashimoto, M. & Uyeda, S.). Terra Scientific Publishing Company, Tokyo, 219–230.

Taira, A. 1981. The Shimanto belt of southwest Japan and arc–trench sedimentary tectonics. *Recent Prog. Nat. Sci. Jap.* **6**, 147–162.

Taira, A., Tashiro, M., Okamura, M. & Katto, J. 1980. The geology of the Shimanto belt in Kōchi Prefecture, Shikoku, Japan. In: *Geology and Paleontology of the Shimanto Belt* (edited by Taira, A. & Tashiro, M.). Rinyakosaikai Press, Tokyo, 319–389.

Taira, A., Oakada, H., Whitaker, J. H. McD. & Smith, A. J. 1982. The Shimanto belt of Japan: Cretaceous–lower Miocene active-margin sedimentation. In: *Trench–Forearc Geology* (edited by Leggett, J. K.). *Spec. Publs geol. Soc. Lond.* **10**, 5–26.

Taira, A., Katto, J., Tashiro, M., Okamura, M. & Kodama, K. 1988. The Shimanto belt in Shikoku, Japan—evolution of Cretaceous to Miocene accretionary prism. *Modern Geol.* **12**, 5–46.

Vissers, R. L. M. 1989. Asymmetric quartz *c*-axis fabrics and flow vorticity: a study using rotated garnets. *J. Struct. Geol.* **11**, 231–244.